Microstructural, structural and optical properties of nanoparticles of $PbO\text{-}CrO_3$ pigment synthesized by a soft route

(Propriedades microestruturais, estruturais e ópticas de nanopartículas de pigmentos de $PbO\text{-}CrO_3$ sintetizadas por rota soft)

V. D. Araújo[1*], M. R. B. Andreeta[2], L. J. Q. Maia[3], R. M. Nascimento[4], F. V. Motta[4], M. R. D. Bomio[4], C. A. Paskocimas[4], M. I. B. Bernardi[5]

[1]Unidade Acadêmica do Cabo de Santo Agostinho, Universidade Federal Rural de Pernambuco - UFRPE, Recife, Brazil 52171-900

[2]Departamento de Engenharia de Materiais, Universidade Federal de S. Carlos - UFSCar, P.O. Box 676, S. Carlos, SP, Brazil 13565-905

[3]Instituto de Física, Universidade Federal de Goiás, Campus Samambaia, C.P. 131, Goiânia, GO, Brazil 74001-970

[4]Laboratório de Síntese Química de Materiais LSQM, DEMat, Universidade Federal do Rio Grande do Norte - UFRN, P.O. Box 1524, Natal, RN, Brazil 59078-970

[5]Instituto de Física de São Carlos, Universidade de S. Paulo - USP, Av. Trabalhador São-carlense 400, S. Carlos, SP, Brazil 13560-970

**vicodantas@yahoo.com.br*

Abstract

$PbCrO_4$ and Pb_2CrO_5 particles were synthesized by the polymeric precursor method. Structural and microstructural properties of the particles were characterized by scanning electron microscopy with field emission gun, X-ray diffraction, and Raman spectroscopy techniques. The diffuse reflectance technique was employed to study the optical properties in the 400-700 nm range. The optical bandgap of the samples was obtained indirectly. Colorimetric coordinates L*, a*, b* were calculated for the pigment powders as a function of the heat treatment (400-700 °C). The powders displayed colors ranging from green to red. X-ray diffraction patterns showed the presence of monoclinic $PbCrO_4$ phase in green samples, while red powders had a monoclinic Pb_2CrO_5 phase structure. The Raman spectra of the $PbCrO_4$ and Pb_2CrO_5 powders were in good agreement with those reported in the literature. The synthesized compounds can be used as green and red pigments with high thermal stability.

Keywords: nanoparticles, $PbCrO_4$, structural properties, microstructural properties, optical properties.

Resumo

Partículas de $PbCrO_4$ and Pb_2CrO_5 foram sintetizadas pelo método do precursor polimérico. Propriedades estruturais e microestruturais das partículas forma caracterizadas por técnicas de microscopia eletrônica de varredura, difração de raios X e espectroscopia Raman. A técnica de refletância difusa foi empregada para o estudo das propriedades ópticas na faixa 400-700 nm. O bandgap óptico foi obtido indiretamente. As coordenadas colorimétricas L, a*, b* foram calculadas para os pós de pigmento em função do tratamento térmico (400-700 °C). Os pós apresentaram cores do verde ao vermelho. Os difratogramas de raios X mostraram a presença da fase $PbCrO_4$ monoclínica nas amostras verdes, enquanto os pós vermelhos apresentaram a fase Pb_2CrO_5 monoclínica. Os espectros Raman dos pós de $PbCrO_4$ e Pb_2CrO_5 estão em concordância com os reportados. Os compostos sintetizados podem ser usados como pigmentos verdes e vermelhos com alta estabilidade térmica.*

***Palavras-chave**: nanopartículas, $PbCrO_4$, propriedades estruturais, propriedades microestruturais, propriedades ópticas.*

INTRODUCTION

In recent years, much attention has focused on nanostructured systems applied in electronic devices or to improve mechanical, chemical, structural, optical, electrical and magnetic properties of materials [1, 2]. Manipulation of the thermodynamic and kinetic control processes plays a key role in crystal growth, which determines the final crystal habit, phase, shape, and structures [3, 4]. The added value of a compound depends on its structural, morphological and optical properties. These properties depend directly on the crystal structure of the material. Thus, studies relating to the material's structure, physical properties, and method of synthesis are essential.

Lead chromate ($PbCrO_4$) is an important solid material that is widely used as a photosensitizer and yellow pigment with a monoclinic P21/n structure [5]. Pb_2CrO_5 was first used as a dielectric material in 1968 [6]. Dilead pentaoxochromate (Pb_2CrO_5) with a monoclinic C2/m structure has a large absorption coefficient and a high-speed photo-response in the visible region of the electromagnetic spectrum. Therefore, it is a potential candidate for application in photoconductors, optoelectronic devices, and reversible thermochromism materials [7]. Pb_2CrO_5 has been found to have wide band gap energy ($E_g \sim 2.1$-2.3 eV) and a large absorption coefficient ($\mu \sim 10^4$ cm^{-1}). The photoresponse and performance of Pb_2CrO_5 devices described in the literature suggest that Pb_2CrO_5 may be classified as a new type of optoelectronic dielectric material that could potentially be used in room temperature photoconductors for the visible and ultraviolet regions [8]. The synthesis of $PbCrO_4$ and Pb_2CrO_5 crystals with well-controlled sizes and shapes is crucial due to their potential applications. The literature describes various procedures to synthesize $PbCrO_4$ and Pb_2CrO_5 crystalline phases into different shapes, such as spherical nanoparticles, nanorods, microparticles, nanowires, rectangular nanorods and nanotubes [7, 9-15]. The reported methods are microemulsion [9], hydrothermal [10, 11], self-seeding template growth (SSTG) process [12], microwave-assisted ionic liquid method [7, 13], and room temperature reaction of solutions without the additives [14].

The polymeric precursor route, the Pechini method, is a nonconventional method of synthesis that offers the advantage of yielding homogeneous systems with a high degree of purity, which can be calcined at relatively low temperatures, allowing the synthesis of nanometric oxides with well defined and controlled properties.

In this work, $PbCrO_4$ and Pb_2CrO_5 crystalline particles, known as crocoites, were synthesized via a soft chemical route, the polymeric precursor method, and the structural, microstructural and optical properties of these crocoites annealed at different temperatures were examined to be used as pigments.

EXPERIMENTAL

The polymeric precursor method is based on the polymerization of metallic citrate using ethylene glycol. A hydrocarboxylic acid such as citric acid is normally used to chelate cations in an aqueous solution. The addition of a polyalcohol such as ethylene glycol leads to the formation of an organic ester. Polymerization promoted by heating to around 100 ºC results a homogenous resin in which the metal ions are distributed uniformly throughout the organic matrix. The resin is then calcined to produce the desired oxides. Lead acetate trihydrate, $(CH_3CO_2)_2Pb{\cdot}3H_2O$, and chromium trioxide, CrO_3, were used as precursors. The lead acetate and chromium trioxide were dissolved in water and then mixed into an aqueous citric acid solution (100 °C) under constant stirring The pH of the solution was adjusted to 1 with nitric acid. Next, ethylene glycol ($HOCH_2CH_2OH$) was added to polymerize the citrate by a polyesterification reaction. The citric acid:metal molar ratio was 6:1, while the citric acid:ethylene glycol mass ratio was 60:40. The Pb:Cr ratio was adjusted in order to obtain two compositions: $PbCrO_4$ and Pb_2CrO_5. The resulting polymeric resin was then calcined to produce the desired oxide. The puff (first calcination) was made at 400 ºC/4 h in an air atmosphere.

After annealing from 500 to 700 °C for 2 h, SEM micrographs of the pigment powders were taken using a Zeiss (DSM-940A) scanning electron microscope equipped with a field emission gun (SEM-FEG), providing larger than 100,000 X magnification.

Raman spectra was recorded with a confocal Raman microscope (WiTec, Alpha 300S – CRM 200) equipped with a piezo scanner and 100 X microscopic objectives (N.A.: 0.90; Nikon, Tokyo, Japan). The spatial resolution in this experiment reached up to 400 nm. Samples were excited with an air-cooled Ar ion laser (Melles Griot, model 35-LAL – 515-230) operating at 514.5 nm with 1 mW of power. Raman data were also obtained on a monochromator equipped with 1800-groove gratings.

The powders were structurally characterized using an automatic X-ray diffractometer (Rigaku, Rotaflex RU200B) with Cukα radiation (50 kV, 100 mA, λ = 1.5405 Å) and in a θ–2θ configuration using a graphite monochromator. The scanning range was between 10 and 75° (2θ), with a step size of 0.02° and a step time of 1 s. The Rietveld analysis was performed with the Rietveld refinement program GSAS [15]. A pseudo-Voigt profile function was used.

The diffuse reflectance and colorimetric coordinates of the pigments were measured using a spectrophotometer (Minolta, CM2600d) in the 400 and 700 nm range, equipped with standard D65 (daylight) light source, following the CIE-L*a*b* colorimetric method recommended by the CIE (Commission Internationale de l'Eclairage) [16]. Other optical property, such as the optical bandgap was obtained indirectly.

RESULTS AND DISCUSSION

The powders obtained in this study presented a broad spectrum of colors ranging from green to red. It known that the colors of some compounds containing transition metals depend on both the structural arrangements of the elements and on the shape and size of the particles. Herewith, we begin this section evaluating the grain size and morphology of the synthesized powders by the SEM-FEG technique.

Fig. 1 presents the SEM-FEG images for the $PbCrO_4$ and Pb_2CrO_5 compositions submitted to different annealing temperatures. Both compositions showed strong particle coalescence forming spherical agglomerates. In the case of $PbCrO_4$, the synthesized particles ranged in size from 500 to 1200 nm, depending on the heat-treatment. The Pb_2CrO_5, in contrast, displayed small grain sizes of 100 to 300 nm. These differences are due to the high reactivity and low sintering energy of $PbCrO_4$ against Pb_2CrO_5, accelerating the grain growth process for $PbCrO_4$.

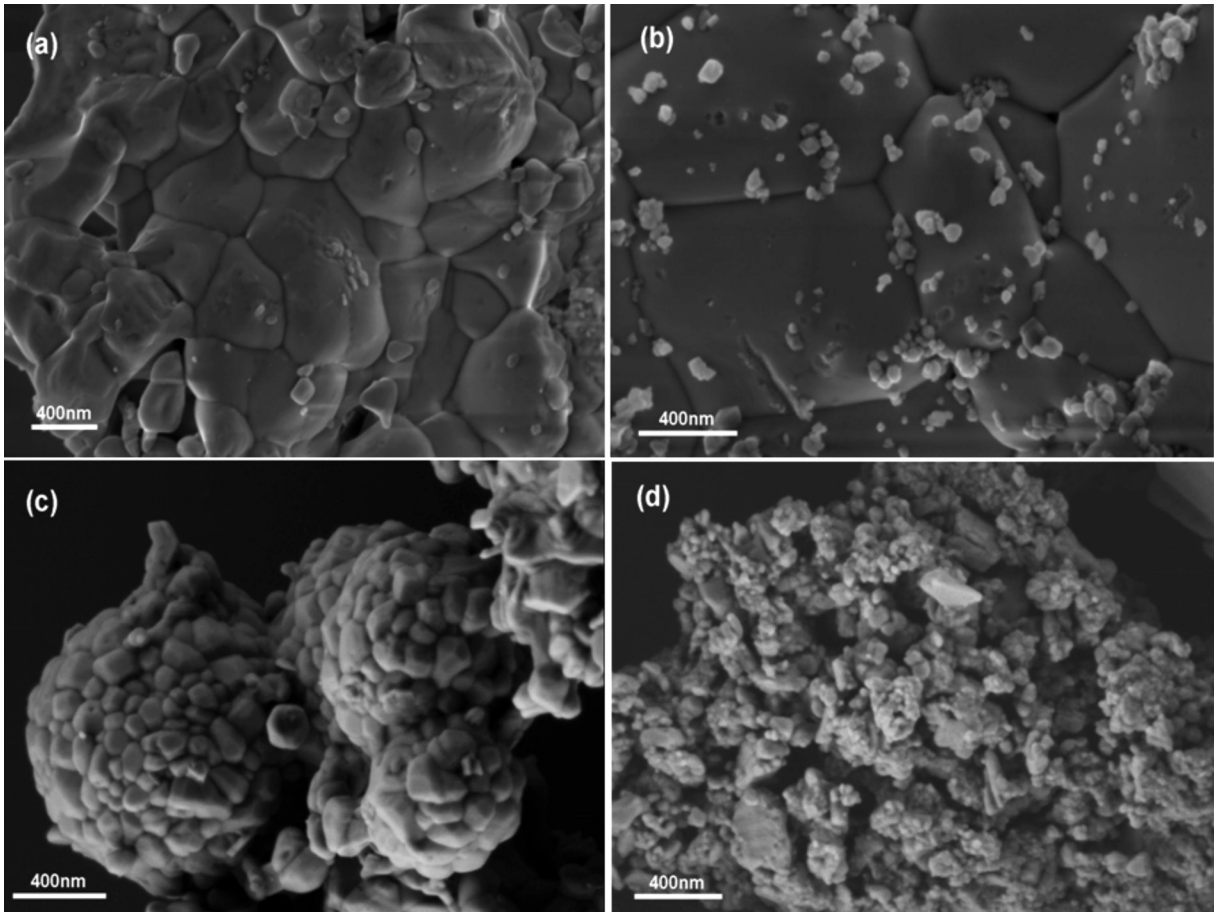

Figure 1: FEG-SEM images of the $PbCrO_4$ (a, b) and Pb_2CrO_5 (c, d) after calcination at 400 °C (a, c) and 700 °C (b, d).
[Figura 1: Imagens obtidas em microscópio eletrônico de varredura de $PbCrO_4$ (a, b) e Pb_2CrO_5 (c, d) após calcinação 400 °C (a, c) e 700 °C (b, d).]

Table I - Raman bands of the samples compared with those reported.
[Tabela I - Bandas Raman das amostras comparadas a valores reportados.]

$PbCrO_4$ [17]	$PbCrO_4$ This work	Pb_2CrO_5 [18]	Pb_2CrO_5 This work	Assignments [17, 18]
853	852	856	850	ν 3
838	837	848	845	ν 1
-	-	839	835	ν 3
825	829	826	823	ν 3
400	401	398	391	ν 4
377	375	377	377	ν 4
359	366	356	353	ν 4
336	344	339	336	ν 2
326	325	322	322	ν 2

Fig. 2 shows the Raman spectra of $PbCrO_4$ and Pb_2CrO_5 samples. According to Wilkins [17] and Frost [18], all vibrational modes of crocoite are Raman-active ($1A_1$ +1E $+2T_2$), but only specimens with T_2 symmetry are IR-active. All degeneracies were removed from the crocoites, resulting in 9A vibrational modes, all Raman- and IR-active. The Cr-O distance in crocoite is around 1.65 Å, indicating a substantial amount of multiple-character bonds in the chromate ion. This leads to strong Raman interactions [17]. The comparative results are presented in Table I, where ν1 and ν3 are the symmetric and asymmetric stretching vibrations of CrO_4^{2-} respectively, ν2 and ν4 are the deformation modes for CrO_4^{2}. Our results were consistent with those of Wilkins [17] and Frost [18], demonstrating the efficiency of the polymeric precursor method to obtain pure $PbCrO_4$ and Pb_2CrO_5 phases. The vibrational modes of Pb_2CrO_5 showed lower frequencies than those of $PbCrO_4$, indicating that the former has a more compact structure which acts as a barrier against

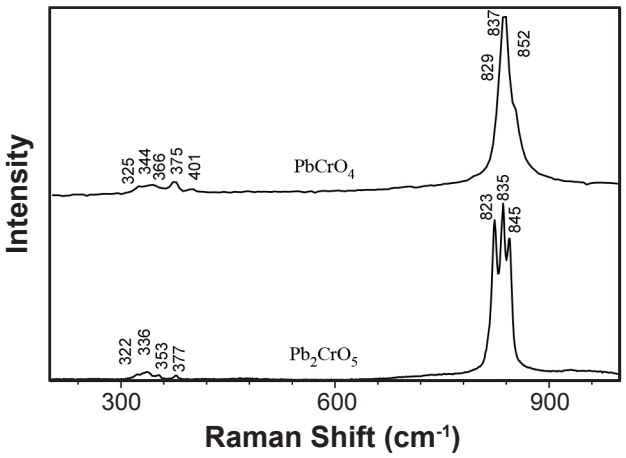

Figure 2: Raman shift spectra of the $PbCrO_4$ and Pb_2CrO_5 nanometric pigment powders synthesized at 700 °C.
[Figura 2: Espectros Raman de pós de pigmentos nanométricos de $PbCrO_4$ e Pb_2CrO_5 sintetizados a 700 °C.]

uncontrolled grain growth. Pb_2CrO_5 therefore has smaller particles than $PbCrO_4$, as illustrated in Fig. 1.

Fig. 3 presents the X-ray diffraction patterns of the $PbCrO_4$ and Pb_2CrO_5 compositions calcined at 400 °C for 4h. The samples annealead at 500 and 600 °C have similar diffraction patterns to the calcined at 400 °C and thus are not presented here. Figs. 4a and 4b show the Rietveld refinement of $PbCrO_4$ and Pb_2CrO_5 samples, respectively. All the reflection peaks in Fig. 4(a) can be indexed easily as $PbCrO_4$ monoclinic phase (space group P21/n (14)) (JCPDS 73-2059), while the peaks in Fig. 4b correspond to Pb_2CrO_5 monoclinic phase (space group C2m (12)) (JCPDS 76-0861).

The refinement parameters, R_{wp}, R_p and R_{Bragg} for the $PbCrO_4$ sample synthesized at 700 °C are 9.71, 6.49 and 3.30 respectively, and for the Pb_2CrO_5 sample 6.74, 4.89 and 1.92 respectively, where R_{wp} and R_p are indicators of the fit quality of the calculated pattern to the observed data and R_{Bragg} monitors the improvement in the structure model, while Table II compares the values of these parameters with those reported in the literature.

The low values of the reliability parameters R_{wp} and R_{Bragg} indicate the good quality of the refinements [19]. An excellent agreement was observed between the unit cell parameters and unit cell volume of the $PbCrO_4$ and Pb_2CrO_5 phases determined from the Rietveld refinements and the values reported in the literature [20, 21]. This statement is also consistent with the Raman results presented earlier.

Following, we present the results and discussions about optical properties of the nanopowders to be applied as pigments. One of the mechanisms responsible for color

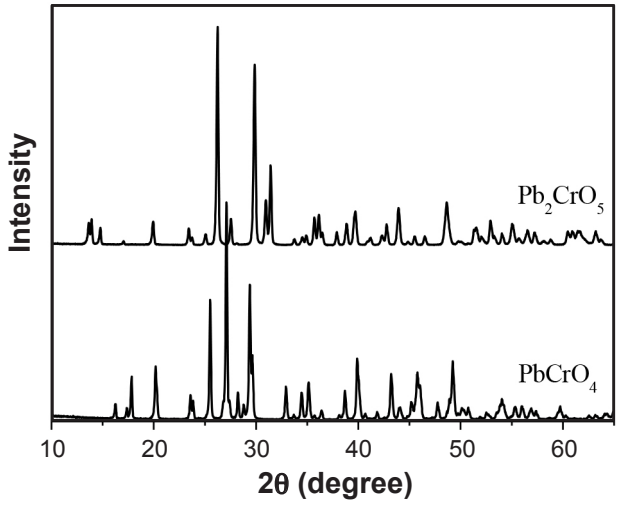

Figure 3: X-ray diffraction patterns of the $PbCrO_4$ and Pb_2CrO_5 after calcination at 400 °C.
[Figura 3: Difratogramas de raios X de $PbCrO_4$ e Pb_2CrO_5 após calcinação a 400 °C.]

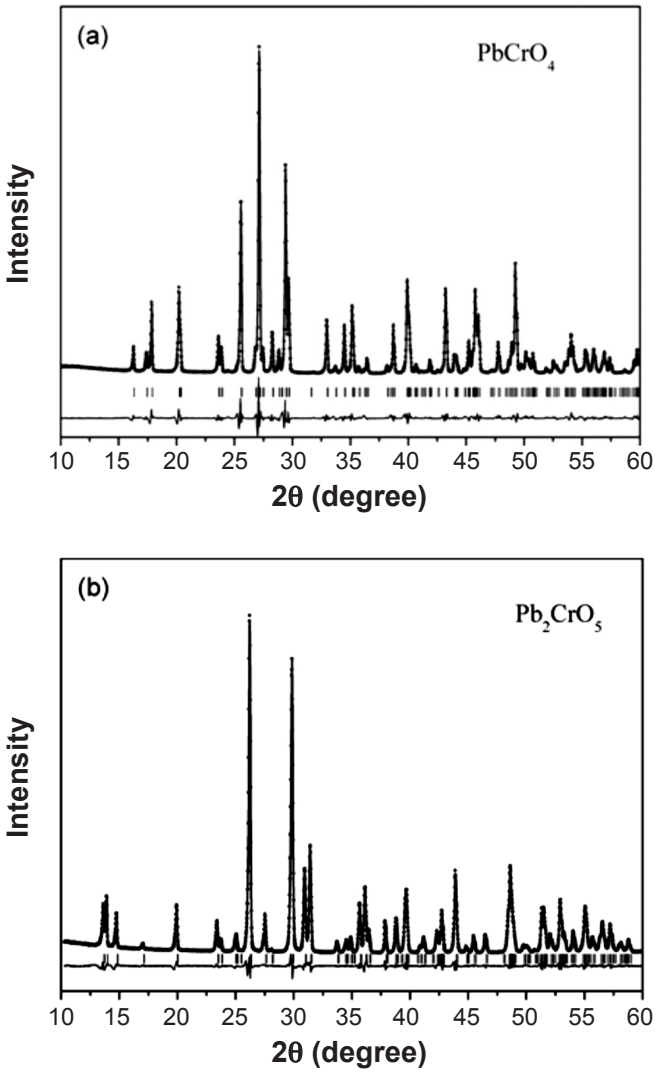

Figure 4: X-ray diffraction patterns and Rietveld refinement of the (a) $PbCrO_4$ and (b) Pb_2CrO_5 after calcination at 700 **°C/2** h.
[Figura 4: Difratogramas de raios X e refinamento de Rietveld de (a) $PbCrO_4$ e (b) Pb_2CrO_5 após calcinação a 700 °C/2 h.]

Table II - Values of Rietveld refinement of $PbCrO_4$ and Pb_2CrO_5 compared with those in the literature.
[Tabela II - Valores de refinamento de Rietveld de $PbCrO_4$ e Pb_2CrO_5 comparados com od publicados.]

Parameters	$PbCrO_4$ Reference (JCPDS 73-2059)	$PbCrO_4$ Refined (this work)
a (Å)	7.12	7.12(7)
b (Å)	7.43	7.43(6)
c (Å)	6.79	6.79(8)
□	90.0°	90.0°
□	102.42°	102.48(9)°
□	90.0°	90.0°
Unit Cell Volume (Å^3)	350.8	351.79°
Z	4	4
Space group	P 21/n	P 21/n
Parameters	Pb_2CrO_5 Reference (JCPDS 76-0861)	Pb_2CrO_5 Refined (This work)
a (Å)	14.001(7)	14.00(3)
b (Å)	5.675(3)	5.67(7)
c (Å)	7.137(5)	7.13(8)
□	90.0°	90.0°
□	115.22°	115.26(3)°
□	90.0°	90.0°
Unit Cell Volume (Å^3)	513.02	513.29
Z	4	4
Space group	C 2/m	C 2/m

generation is known as charge transfer. This mechanism, which consists of the motion of an electron from one transition metal ion to another, produced by the absorption of light energy [22], is responsible for the color of $PbCrO_4$ and Pb_2CrO_5 compounds. Highly charged ions such as Cr^{6+} are not favored energetically. Cr^{6+} ions exert a strong attraction on electrons, and the movement of some fraction of one or more electrons from the oxygen back to the central ions produces a much more stable arrangement, resulting in ligand-to-metal (anion-to-cation) charge transfer transitions and the color of both compounds. For $PbCrO_4$ and Pb_2CrO_5, the result is a broad absorption band at blue and high transmittance for the other wavelengths, leading to an green color for $PbCrO_4$ and a red color for Pb_2CrO_5 [23].

Fig. 5 shows the diffuse reflectance of $PbCrO_4$ and Pb_2CrO_5 powders. The diffuse reflectance spectra indicate that absorption bands in the 560 nm region of $PbCrO_4$ (a green powder) and 400-550 nm of Pb_2CrO_5 (a red powder) redshift as the annealing temperature increases, as illustrated in Figs. 5a and 5b.

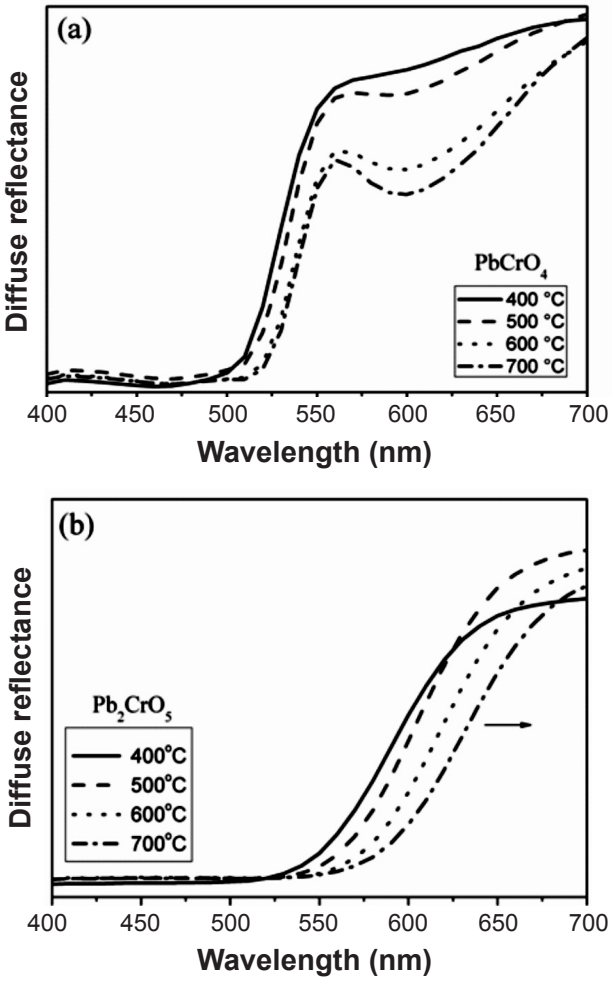

Figure 5: Diffuse reflectance spectra of a) $PbCrO_4$, and b) Pb_2CrO_5 calcined at different temperatures.
[Figura 5: Espectros de refletância difusa de a) $PbCrO_4$ e b) Pb_2CrO_5 calcinados a diferentes temperaturas.]

The three absorption bands in Fig. 5a for $PbCrO_4$ at around 400, 500 and 600 nm are in agreement with those observed by Reddy et al [24]. The first two bands are assigned to the transitions $1t_1 \rightarrow 2e$, $6t_2 \rightarrow 2e$ respectively, and the band at 600 nm might be due to a forbidden transition.

It is well known that the morphology and size of materials have important effects on their color [25-27]. We believe that the red shift in diffuse reflectance in Fig. 6 may be attributed to small differences in particle size and shape with increasing annealing temperature as can be seen in Fig. 1.

Color can be measured by several methods, but in ceramics, the most common method to determine the color of a product is the CIE-L*a*b* [17]. This method measures the intensity of diffuse reflectance in the visible region to obtain the three colorimetric coordinates L*, a*, b*, yielding the black/white lightness, green/red and blue/yellow color intensities, respectively, as well as the total color difference, ΔE. This parameter ΔE is defined as the total color difference between the studied material and a reference sample, i.e., $\Delta E^2 = \Delta L^{*2} + \Delta a^{*2} + \Delta b^{*2}$. For each correspondent composition, the sample calcined

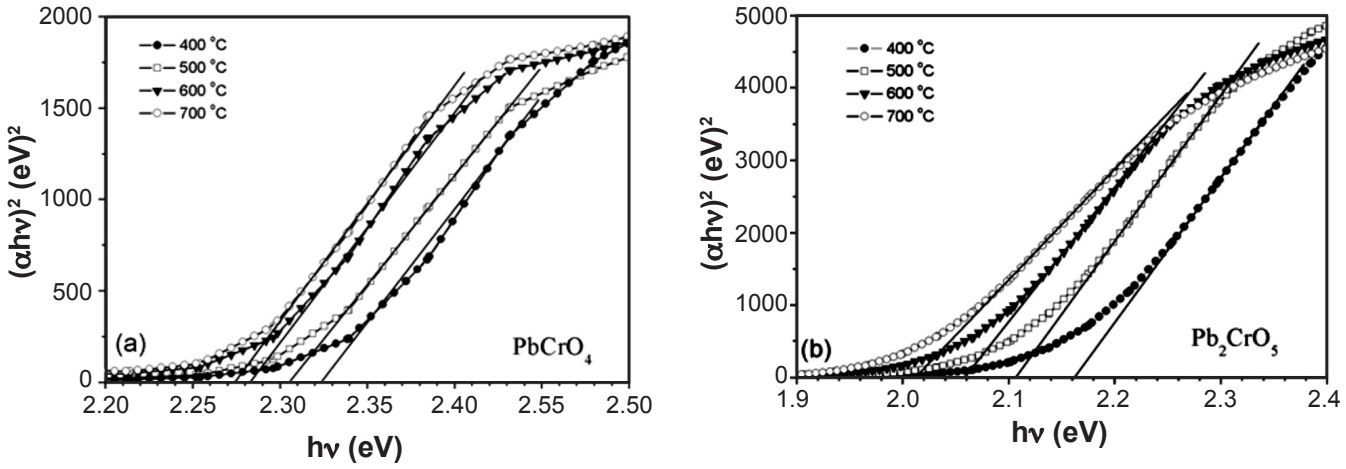

Figure 6: Absorption coefficient as a function of incident photon energy in the near band gap region of $PbCrO_4$ (a) and Pb_2CrO_5 (b) powders calcined at different temperatures.
*[Figura 6: Coeficiente de absor*ção em função da energia do fóton incidente na região próxima do bandgap de pós de $PbCrO_4$ *(a) e Pb_2CrO_5 calcinados em diferentes temperaturas.]*

Table III - Colorimetric coordinates (a*, b* and L*), total color difference (ΔE) of $PbCrO_4$ and Pb_2CrO_5, using type D65 (daylight) light source, following the CIE-L*a*b* standard colorimetric method, and the optical bandgap of the powders as a function of the heat treatment.
[Tabela III - Coodenadas colorimétricas (a, b* e c*) diferença de cor total (ΔE) de $PbCrO_4$ e Pb_2CrO_5, usando fonte de luz (luz do dia) D65, segundo o método colorimétrico padrão CIE-L*a*b*, e o bandgap óptico dos pós em função do tratamento térmico.]*

Sample – Calcination Temperature	Light Source	a*	b*	L*	ΔE	E_g (± 0.05 eV)
$PbCrO_4$ – 400°C	D65-10°	10.07	38.17	43.91	-	2.32
$PbCrO_4$ – 500°C	D65-10°	11.06	33.75	42.73	4,68	3.31
$PbCrO_4$ – 600°C	D65-10°	10.61	27.86	37.49	12,16	2.28
$PbCrO_4$ – 700°C	D65-10°	10.26	26.85	37.70	12,91	2.27
Pb_2CrO_5 – 400°C	D65-10°	42.25	49.93	44.92	-	2.16
Pb_2CrO_5 – 500°C	D65-10°	41.26	36.24	41.36	14,18	2.11
Pb_2CrO_5 – 600°C	D65-10°	35.99	31.17	40.41	20,28	2.06
Pb_2CrO_5 – 700°C	D65-10°	33.78	28.02	38.53	24,34	2.01

at 400 °C for 4 h was used as reference. Table III presents the colorimetric coordinates (L*, a*, b*) and total color difference (ΔE) of $PbCrO_4$ and Pb_2CrO_5 nanoparticles obtained in this work, using type D65-10° (day light) light source determined by the CIE-L*a*b* standard colorimetric method.

The samples' colorimetric values a*, b* and L* reduced as the calcination temperature was increased, indicating that their red color enhanced by increasing the temperature. We believe that these changes are related to differences in particle size as the annealing temperature increases, as shown for the diffuse reflectance above. It is related to defects on the as prepared surface nanoparticles. The defects on crystalline surface nanoparticles are reduced, once the crystallinity increased with the temperature as showed by DRX results.

Other optical property, such as the optical bandgap was obtained indirectly. Considering the high absorption region, the transmittance *T* and reflectance *R* followed a simplecorrelation with absorption coefficient:

$$T = A \exp(-\lambda d) \quad \text{(A)}$$

where *A* is approximately equal to the unity at the absorption edge and *d* is the thickness of the sample. The relation between the absorption coefficient λ and incident photon energy *h*ν for allowed direct transition can be written as [28, 29]

$$\Delta h\nu = A_1 (h\nu - E_g)^{1/2} \quad \text{(B)}$$

where A_1 is a constant and E_g is the direct bandgap.

The $(\Delta h\nu)^2$ vs. $h\nu$ plots for the powders calcined at different temperatures are shown in Fig. 6. A linear behavior

can be observed in a certain range of the curves, supporting the interpretation of direct E_g band gap for powders [28, 29]. Therefore, the E_g bandgap of the powders can be obtained by extrapolating relation (B) between 2.32 eV and 2.27 eV for $PbCrO_4$ and 2.16 eV and 2.01 eV for Pb_2CrO_5. Table III gives the optical bandgap values determined from Figure 6. As can be seen, the band gap of powders decreases from 2.32 eV to 2.27 eV for $PbCrO_4$ and from 2.16 eV to 2.01 eV for Pb_2CrO_5 as the heat treatment increases from 400 °C to 700 °C. Elevating the treatment temperature, increase powder crystallinity and reduces bandgap, thus increasing the conductive nature of compounds.

Lu *et al* [30] have observed that change in energy gap with the grain size of $BaTiO_3$ films must have a close relation to the interatomic spacing (lattice parameters). Also, they have mentioned that the decrease in bandgap value on annealing (amorphous → microcrystalline) might be due to the lowering of the interatomic spacing, which reduced the polarization and electron-hole interaction corrections. Certainly, similar effects occur in our synthesized crocoites powders. Once that the crystallinity increases with the annealing, and at 700 °C we have well crystallized powders with lattice parameters close to those reported in literature, Table II. Then, the color changes can be attributed to the crystallinity degree and the optical bandgap. It seems that for Pb_2CrO_5 powder, the color changes are directly related to the optical bandgap displacement. About the $PbCrO_4$ compound, the color changes are related to two factors: the optical band gap and the band centered around 600 nm (Fig. 5a).

CONCLUSIONS

The polymeric precursor method proved efficient to synthesize pigments with colors ranging from green to red, since it yielded pure $PbCrO_4$ and Pb_2CrO_5 phases. The reflectance and colorimetric measurements showed that the $PbCrO_4$ samples presented varying shades of green to mustard, while the color of the Pb_2CrO_5 samples ranged from orange to red. The Raman spectra were congruous with the X-ray diffraction patterns, indicating the presence of $PbCrO_4$ and Pb_2CrO_5 in the samples. Moreover, the bands detected were compatible with those reported. The samples displayed strong coalescence and considerable particle agglomeration. The colors of the synthesized pigments were correlated with the type of phase present in each sample, as well as the particle size, the crystallinity degree and the optical bandgap.

ACKNOWLEDGEMENTS

The authors gratefully acknowledge the financial support of the Brazilian research funding agencies FAPESP, CNPq, PRONEX/FINEP and CAPES.

REFERENCES

[1] C. Burda, X. B. Chen, R. Narayanan, M.A. El-Sayed. Chem. Rev. **105** (2005) 1025-1102.
[2] T. L. Porter, M. E. Hagerman, B. P. Reynolds, M. P. Eastman, R. A. Parnell, J. Polym. Sci. Part B-Polym. Phys. **36** (1998) 673-679.
[3] H. Cölfen, S. Mann. Angew. Chem., Int. Ed. **42** (2003) 2350-2365.
[4] S. R. Dickinson, K. M. McGrath. J. Mat. Chem. **13** (2003) 928-933.
[5] K. Toda, S. Watanabe. J. Mat. Sci. Lett. **18** (1999) 689-690.
[6] N. Yukami, M. Ikeda, Y. Harada, M. Nisitani, T. Nishikura. IEEE Trans. Electron Dev. **33** (1986) 520-525.
[7] W. W. Wang, Y. J. Zhu. Cryst. Growth Des. **5** (2005) 505-507.
[8] K. A. Wishah, M. M. Abdul-Gader. Appl. Phys. A: Mater. Sci. Process. **66** (1998) 229-234.
[9] A. K. Panda, B. B. Bhowmik, A. R. Das, S. P. Moulik. Langmuir **17** (2001) 1811-1816.
[10] J. Liang, Y. Li, J. Cryst. Growth **261** (2004) 577-580.
[11] X. L. Hu, Y. J. Zhu, Chem. Lett. **33** (2004) 880-881.
[12] D. Chen, K. Tang, Z. Liang, Y. Liu, H. Zheng, Nanotechnology **16** (2005) 2619-2624.
[13] Y. J. Zhu, W. W. Wang, R. J. Qi, X. L. Hu, Angew. Chem., Int. Ed. **43** (2004) 1410-1414.
[14] J. H. Xiang, S. H. Yu, Z. Xu, Cryst. Growth Des. **4** (2004) 1311-1315.
[15] A. C. Larson, R. B. Von Dreele, Los Alamos National Laboratory, Los Alamos, EUA, Copyright, 1985–2000, The Regents of the University of California (2001).
[16] CIE, "Recommendations of uniform color spaces, color difference equations, phychometrics color terms", Suppl. 2 CIE Publ. 15 (E1e1.31) (1971), Bureau Central de la CIE, Paris, France (1978).
[17] R. W. T. Wilkins, Mineral. Mag. **38** (1971) 249-250.
[18] R. L. Frost, J. Raman Spectrosc. **35** (2004) 153-158.
[19] M. L. Moreira, G. P. Mambrini, D. P. Volanti, E. R. Leite, M. O. Orlandi, P. S. Pizani, V. R. Mastelaro, C. O. Paiva-Santos, E. Longo, J. A. Varela, Chem. Mater. **20** (2008) 5381-5387.
[20] S. Quareni, R. De Pieri, Rend. Soc. Mineral. Ital. **20** (1964) 235-250.
[21] S. A. Williams, W. J. McLean, J. W. Anthony, Am. Mineral. **55** (1970) 784-792.
[22] K. Nassau, "The Physics and Chemistry of color", Wiley Intersci. Publ., New York, USA (2001).
[23] K. Nassau, Am. Mineral. **63** (1978) 219-229.
[24] B. J. Reddy, K. B. N. Sarma, Phys. Lett. **86A** (1981) 386-388.
[25] M. Quinten, Appl. Phys. B **73** (2001) 317-326.
[26] J. Wang, W. B. White, J. H. Adair, J. Am. Ceram. Soc. **88** (2005) 3449-3454.
[27] L. J. R. Marshall, J. R. Williams, M. J. Almond, S. D. M. Atkinson, S. R. Cook, W. Matthews, J. L. Mortimore, Spectrochim. Acta, Part A **61** (2006) 233-241.
[28] L. J. Q. Maia, M. I. B. Bernardi, C. A. C. Feitosa, V. R. Mastelaro, A. R. Zanatta, A. C. Hernandes, Thin Solid Films **457** (2004) 246-252.
[29] A. J. Barbosa, F. A. Dias Filho, L. J. Q. Maia, Y.

Messaddeq, S. J. L. Ribeiro, R. R. Gonçalves. J. Phys.: Condens. Matter **20** (2008) 285224.

[30] X. M. Lu, J. S. Zhu, W. Y. Zhang, G. Q. Ma, Y. N. Wang, Thin Solid Films **274** (1996) 165-168.
(Rec. 10/07/2014, Rev. 08/09/2014, Ac. 12/01/2015)